Supplementary Information: Thermally Driven Ratchet Motion of Skyrmion Microcrystal and Topological Magnon Hall Effect

M. Mochizuki[1,2],*, X. Z. Yu[3], S. Seki[2,3,4], N. Kanazawa[5], W. Koshibae[3], J. Zang[6], M. Mostovoy[7], Y. Tokura[3,4,5], and N. Nagaosa[3,4,5]

[1] *Department of Physics and Mathematics,*

Aoyama Gakuin University, Sagamihara, Kanagawa 229-8558, Japan

[2] *PRESTO, Japan Science and Technology Agency,*

Kawaguchi, Saitama 332-0012, Japan

[3] *RIKEN Center for Emergent Matter Science (CEMS), Wako, Saitama 351-0198, Japan*

[4] *Department of Applied Physics, Quantum-Phase Electronics Center,*

The University of Tokyo, Bunkyo-ku Tokyo 113-8656, Japan

[5] *Department of Applied Physics, The University of Tokyo,*

Bunkyo-ku, Tokyo 113-8656, Japan

[6] *Department of Physics and Astronomy,*

Johns Hopkins University, Baltimore, Maryland 21218, USA and

[7] *Zernike Institute for Advanced Materials,*

University of Groningen, Nijenborgh 4,

9747 AG, Groningen, The Netherlands

---
*Electronic address: mochizuki@phys.aoyama.ac.jp

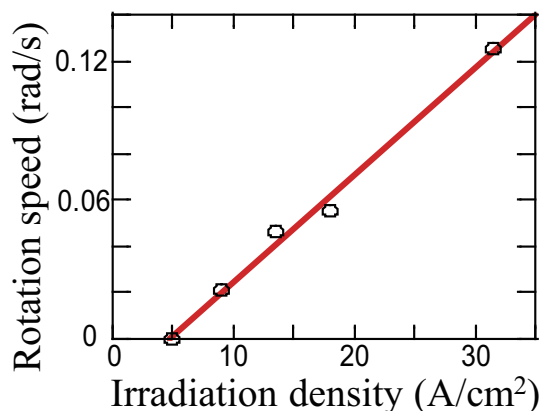## I. ROTATION RATE AS A FUNCTION OF THE ELECTRON-BEAM INTENSITY

FIG. S1: Rotation rate as a function of irradiation density of the electron beam. The rotation occurs only above a critical irradiation density and its speed increases monotonically, indicating that the observed chiral rotation is a nonequilibrium phenomenon. The red line is a guide for the eyes.

We have studied dependence of rotation rate on irradiation density of the electron beam. Figure S1 shows that the rotation rate increases with increasing irradiation density above a threshold value. These measurements have been performed at a relatively low temperature, T=6 K, because they show a clearer intensity dependence than high-temperature measurements. At T=6 K the electron beam intensity needed to produce the rotation is much higher (by nearly three orders of magnitude) than the value given in the main text.

II. THEORETICAL PHASE DIAGRAM

The phase diagram of the model (1) in the main text has been studied by combining the Monte-Carlo technique with the numerical relaxation using the Landau-Lifshitz-Gilbert (LLG) equation. We first performed the replica-exchange Monte-Carlo calculations to obtain magnetic structures at low temperatures. Then we further relaxed them at T=0 in the numerical calculation of the LLG equation. Comparing the energies of thus prepared magnetic configurations, we obtained the phase diagram as a function of the magnetic field
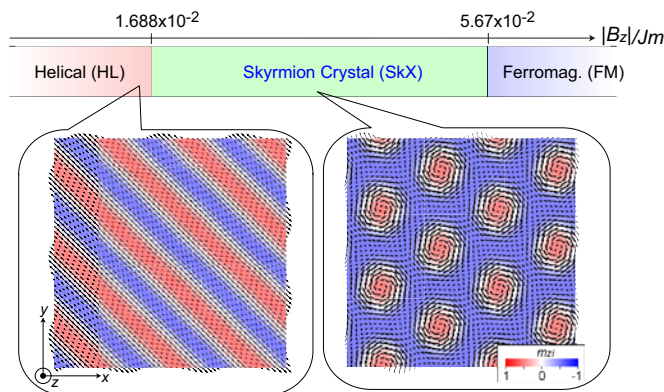
FIG. S2: Theoretically obtained magnetic phase diagram of the model (1) in the main text as a function of magnetic field B_z at $T=0$.

B_z shown in Fig.S2. Helical (HL), skyrmion-crystal (SkX), and ferromagnetic (FM) phases emerge successively as the field strength $|B_z|$ increases.

III. MAGNON-DRIVEN SKYRMION DYNAMICS

Here we sketch the derivation of equations of motion for the center-of-mass coordinates of a skyrmion. We consider a continuum model describing the unit vector $\boldsymbol{n}(\boldsymbol{r}, t)$ in the spin direction, which is related to the magnetization vector, $\boldsymbol{m}_i$, defined at the lattice sites as $\boldsymbol{n}(\boldsymbol{r}_i) = -\boldsymbol{m}_i/m$. The Lagrangian of the model is

$$\mathcal{L} = S \int d\boldsymbol{r} (\cos\theta - 1)\dot{\phi} - \mathcal{H}, \tag{S1}$$

where the first term is the Berry phase expressed through the polar angles θ and ϕ: $\boldsymbol{n} = (\sin\theta\cos\phi, \sin\theta\sin\phi, \cos\theta)$, while the second term is the spin Hamiltonian,

$$\mathcal{H} = \int d\boldsymbol{r} \left[\frac{JS^2}{2} \sum_\alpha (\partial_\alpha \boldsymbol{n})^2 + DS^2 \boldsymbol{n} \cdot [\nabla \times \boldsymbol{n}] + S\boldsymbol{B} \cdot \boldsymbol{n} \right]. \tag{S2}$$

Here we set the lattice constant a and $\hbar$ to unity.

Skyrmion equations of motion can be understood in terms of conservation of the total momentum,

$$\boldsymbol{P} = -\int d\boldsymbol{r} \frac{\delta\mathcal{L}}{\delta\dot{\phi}} \nabla\phi = S \int d\boldsymbol{r} (1 - \cos\theta) \nabla\phi. \tag{S3}$$

For $\boldsymbol{n}(\boldsymbol{r}, t) = \boldsymbol{n}_0(\boldsymbol{r} - \boldsymbol{R}(t)) + \boldsymbol{n}_1 + \delta\boldsymbol{n}$, where the first term is the rigid skyrmion texture displaced by $\boldsymbol{R} = (X, Y)$, the second term is the deformation of a moving skyrmion

proportional to $\dot{\boldsymbol{R}}$ and the last term describes spin waves, we obtain

$$P_\alpha = 4\pi QS \varepsilon_{\alpha\beta} R_\beta + \mathcal{M} \dot{R}_\alpha + P_\alpha^{\text{magnon}}. \tag{S4}$$

The first two terms represent the skyrmion momentum. Here, $Q = \pm 1$ is the skyrmion topological charge, $\varepsilon_{\alpha\beta}$ is the antisymmetric tensor and $\mathcal{M} = \frac{S}{2}\int d\boldsymbol{r}\, \boldsymbol{n}_0 \cdot \left[\frac{\partial \boldsymbol{n}_1}{\partial \dot{R}_\alpha} \times \frac{\partial \boldsymbol{n}_0}{\partial r_\alpha} \right]$ is the skyrmion mass. The last term in Eq.(S4) is the momentum carried by magnons.

Equations of motion for a skyrmion have then the form:

$$\begin{cases} \mathcal{M}\ddot{X} + \alpha_{\text{G}}\Gamma\dot{X} + 4\pi QS\dot{Y} = F_x, \\ \mathcal{M}\ddot{Y} + \alpha_{\text{G}}\Gamma\dot{Y} - 4\pi QS\dot{X} = F_y, \end{cases} \tag{S5}$$

where the force acting on the skyrmion is $\boldsymbol{F} = -\dot{\boldsymbol{P}}^{\text{magnon}} - \frac{\partial U}{\partial \boldsymbol{R}}$. Here we took into account the external potential $U(\boldsymbol{R})$, describing the repulsion of skyrmions from the disk edge, as well as the friction force resulting from the Gilbert damping, α_{G} being the damping constant and $\Gamma = S \int d\boldsymbol{r}\, \partial_\alpha \boldsymbol{n}_0 \cdot \partial_\alpha \boldsymbol{n}_0 \approx 5.577\pi S$.

Next we show that the skyrmion induces a unit flux of an effective magnetic field acting on magnons, in the same way it does for spin-polarized electrons [S1]. The effective magnetic field originates from the orthogonality of $\delta\boldsymbol{n}$ describing spin waves to the skyrmion texture $\boldsymbol{n}_0$: $\delta\boldsymbol{n}(\boldsymbol{r}, t) = \psi_1(\boldsymbol{r}, t)\boldsymbol{e}_1(\boldsymbol{r}) + \psi_2(\boldsymbol{r}, t)\boldsymbol{e}_2(\boldsymbol{r})$, where $(\boldsymbol{e}_1, \boldsymbol{e}_2, \boldsymbol{n}_0)$ form an orthonormal basis. The freedom in the choice of $\boldsymbol{e}_1(\boldsymbol{r})$ and $\boldsymbol{e}_2(\boldsymbol{r})$ at different $\boldsymbol{r}$, $\boldsymbol{e}_1(\boldsymbol{r}) + i\boldsymbol{e}_2(\boldsymbol{r}) \rightarrow e^{i\chi(\boldsymbol{r})}(\boldsymbol{e}_1(\boldsymbol{r}) + i\boldsymbol{e}_2(\boldsymbol{r}))$, corresponds to the gauge transformation of the magnon wave function, $\psi = \psi_1 + i\psi_2 \rightarrow e^{i\chi}\psi$. It gives rise to the effective gauge potential $a_\alpha = \boldsymbol{e}_1 \cdot \partial_\alpha \boldsymbol{e}_2$ in the magnon Hamiltonian:

$$\mathcal{H}_{\text{magnon}} = \frac{JS^2}{2}\int d\boldsymbol{r} \left[(\hat{P}_\alpha \psi)^\dagger (\hat{P}_\alpha \psi) + \ldots \right], \tag{S6}$$

where $\hat{P}_\alpha = -i\partial_\alpha - a_\alpha - \frac{D}{J}(n_0)_\alpha$. Here we assume that $k_{\text{B}}T \gg D^2/J$, in which case the typical de Broglie wave length of thermal magnons, $2\pi/k$, is much smaller than the skyrmion radius $R_{\text{s}} \sim J/D$, which allows us to omit the k^0 terms in Eq.(S6). The magnon Hamiltonian has essentially the same form as the Hamiltonian of spin-polarized electrons moving through the skyrmion texture and the flux of the effective magnetic field $h_z = \partial_x a_y - \partial_y a_x$ induced by the skyrmion, $\int d\boldsymbol{r} h_z = 4\pi Q$, is twice the flux acting on spin-polarized electrons [S1]. This effective magnetic field gives rise to the "magnon Lorentz force"

$$m^{\text{magnon}}\frac{d\boldsymbol{v}}{dt} = \boldsymbol{v} \times \boldsymbol{h}. \tag{S7}$$

where $\boldsymbol{v}$ is the magnon velocity and $m^{\text{magnon}} = \frac{1}{2JS}$ is the magnon mass in the free-magnon dispersion $\varepsilon_k = JSk^2 + |B_z|$. For $Q = -1$, the sign of h_z is negative and the magnons driven by the temperature gradient $-\frac{\partial T}{\partial x} > 0$ in the x-direction scatter in the positive y-direction. This skew scattering results in the counterclockwise rotation of magnons in the disk (the vector potential due to the Dzyaloshinskii-Moriya interaction $\propto (n_0)_\alpha$ as well as the k^0 terms in the Hamiltonian (S6) do not lead to the magnon rotation).

The skew scattering of magnons exerts the reaction force $F_y = -\dot{P}_y^{\text{magnon}}$ on skyrmions equal the product of the effective magnetic field flux and the magnon current in the x direction:

$$-\dot{P}_y^{\text{magnon}} = 4\pi Q J_x^{\text{magnon}} \tag{S8}$$

(and similarly, $-\dot{P}_x^{\text{magnon}} = -4\pi Q J_y^{\text{magnon}}$). This reaction force induces the observed clockwise rotation of skyrmions.

Equation (S8) can be derived using the close analogy between the magnon and electron transports through the skyrmion crystal. The set of Euler-Lagrange equations for the center-of-mass coordinates of skyrmions coupled to magnons,

$$\begin{cases} \mathcal{M}\ddot{X} + \alpha_{\text{G}}\Gamma\dot{X} + 4\pi Q\left(S\dot{Y} + J_y^{\text{magnon}}\right) = -\frac{\partial U}{\partial X}, \\ \mathcal{M}\ddot{Y} + \alpha_{\text{G}}\Gamma\dot{Y} - 4\pi Q\left(S\dot{X} + J_x^{\text{magnon}}\right) = -\frac{\partial U}{\partial Y}, \end{cases} \tag{S9}$$

where

$$\boldsymbol{J}^{\text{magnon}} = -\frac{\delta\mathcal{H}}{\delta\boldsymbol{a}} = \frac{JS^2}{2}\left[\psi^*\hat{\boldsymbol{P}}\psi + \text{h.c.}\right] \tag{S10}$$

is the average magnon current density, has the same form as the equations of motion for skyrmions driven by the electrical current [S1]. The skew scattering of magnons off skyrmions is analogous to the Topological Hall Effect of electrons observed in MnSi [S2, S3]. However, it is noted that the Hall angle for magnons can be much larger than that for electrons, because the magnon wavelength can be comparable to the size of the skyrmion, whereas the electron wavelength is much shorter.

In numerical simulation, it is difficult to define the rotated frames $\boldsymbol{e}_1$, $\boldsymbol{e}_2$, and $\boldsymbol{n}_0$. Therefore, instead, we have calculated the following current density,

$$J_\mu = \frac{1}{2}\left[z_1^\dagger(-i\partial_\mu - a_\mu - \frac{D}{J}\sigma_\mu)z_1 + \text{h.c.}\right], \tag{S11}$$

$$a_\mu = -i\left[z_0^\dagger\partial_\mu z_0 - \partial_\mu z_0^\dagger z_0\right]. \tag{S12}$$

Here we introduce a two-component complex variable $z =^T (z_\uparrow, z_\downarrow)$ with $z_\uparrow = \cos(\theta/2)$ and $z_\downarrow = e^{i\phi}\sin(\theta/2)$, which represents $\boldsymbol{S}$ as $\boldsymbol{S} = S z^\dagger \boldsymbol{\sigma} z$ with $\boldsymbol{\sigma} = (\sigma_x, \sigma_y, \sigma_z)$ being the Pauli matrices. The spin configuration $z(\boldsymbol{r}, t)$ is composed of two contributions as $z(\boldsymbol{r}, t) = z_0(\boldsymbol{r} - \boldsymbol{R}(t)) + z_1(\boldsymbol{r} - \boldsymbol{R}(t))$ where $z_0(\boldsymbol{r} - \boldsymbol{R}(t))$ represents the rigid skyrmion solution with its core at $\boldsymbol{R}(t)$, while $z_1(\boldsymbol{r} - \boldsymbol{R}(t))$ represents deviations from the rigid configuration due to magnon excitations. This expression contains both contributions from magnons and skyrmions. However, as seen in Fig. 4a in the main text, $\boldsymbol{J}(\boldsymbol{r})$ is small inside the skyrmions, and hence we can regard $\boldsymbol{J}(\boldsymbol{r})$ as $\boldsymbol{J}_i^{\mathrm{magnon}}$ outside of the skyrmions.

IV. ROTATION OF SKYRMION CRYSTAL

Equations of motion (S9) have an obvious generalization to N_S-skyrmion problem. Multiplying the first equation by X_n and the second equation by Y_n (here the index $n = 1, \ldots, N_\mathrm{S}$ labels skyrmions), adding the resulting equations and taking time average, we obtain

$$\left\langle \sum_n \left(\boldsymbol{R}_n \cdot \frac{\partial U}{\partial \boldsymbol{R}_n} - \mathcal{M}\dot{\boldsymbol{R}}_n^2 \right) \right\rangle + 4\pi Q \left\langle \sum_n \boldsymbol{R}_n \times \left(S\dot{\boldsymbol{R}}_n + \boldsymbol{J}^{\mathrm{magnon}}(\boldsymbol{R}_n) \right) \right\rangle = 0, \quad \text{(S13)}$$

where we made use of the fact that the average of a total time derivative is zero. The first average in Eq.(S13) vanishes due to virial theorem. Hence,

$$\left\langle \sum_n \boldsymbol{R}_n \times \dot{\boldsymbol{R}}_n \right\rangle = -\frac{1}{S} \left\langle \sum_n \boldsymbol{R}_n \times \boldsymbol{J}^{\mathrm{magnon}}(\boldsymbol{R}_n) \right\rangle, \quad \text{(S14)}$$

from which we obtain the estimate for the SkX rotation rate,

$$\nu = \frac{1}{2\pi} \left\langle \frac{\sum_n \boldsymbol{R}_n \times \dot{\boldsymbol{R}}_n}{\sum_n \boldsymbol{R}_n^2} \right\rangle \sim \frac{1}{\pi SR} \frac{1}{N_\mathrm{S}} \left\langle \sum_n \frac{\boldsymbol{R}_n \times \boldsymbol{J}^{\mathrm{magnon}}(\boldsymbol{R}_n)}{|\boldsymbol{R}_n|} \right\rangle. \quad \text{(S15)}$$

[S1] Zang, J., Mostovoy, M., Han, J. H., & Nagaosa, N. Dynamics of Skyrmion Crystals in Metallic Thin Films. *Phys. Rev. Lett.* **107**, 136804 (2011).

[S2] Lee, M., Kang, W., Onose, Y., Tokura, Y., & Ong, N. P., Unusual Hall Effect Anomaly in MnSi under Pressure. *Phys. Rev. Lett.* **102**, 186601 (2009).

[S3] Neubauer, A., Pfleiderer, C., Binz, B., Rosch, A., Ritz, R., Niklowitz, P. G., & Böni, P. Topological Hall Effect in the A Phase of MnSi. *Phys. Rev. Lett.* **102**, 186602 (2009).